Characterization of Regular and Plugged SBA-15 Silicas by Using Adsorption and Inverse Carbon Replication and Explanation of the Plug Formation Mechanism

Michal Kruk,[†] Mietek Jaroniec,*[,†] Sang Hoon Joo,[‡] and Ryong Ryoo*[,‡]

Department of Chemistry, Kent State University, Kent, Ohio 44242, and National Creative Research Initiative Center for Functional Nanomaterials, and Department of Chemistry (School of Molecular Science-BK21), Korea Advanced Institute of Science and Technology, Daejeon, 305-701, Korea

Received: October 7, 2002; In Final Form: January 8, 2003

A series of SBA-15 silicas was synthesized using triblock copolymer templates with the same length of poly(propylene oxide) block (PO_m; $m = 70$) and different average lengths of poly(ethylene oxide) blocks (EO_n, $n = 17-28$). The average EO_n length was varied by mixing $EO_{20}PO_{70}EO_{20}$ copolymer with either $EO_5PO_{70}EO_5$ or $EO_{106}PO_{70}EO_{106}$ copolymer, whereas the tetraethyl orthosilicate (TEOS)/EO-unit molar ratio was kept constant. In addition, samples with the higher ratios were synthesized for the $EO_{20}PO_{70}EO_{20}$ template. In all cases, 2-D hexagonally ordered SBA-15 silicas with interconnected primary pore structure (as inferred from carbon inverse replication) were obtained, but higher TEOS/EO-unit molar ratios resulted in the formation of samples with plugged pore structures, which were recently reported by others and referred to as plugged hexagonal templated silicas (PHTSs). Nitrogen adsorption data showed that *n* equal to about 19 was optimal from the point of view of formation of high-pore-volume, large-pore SBA-15 structure. All of the replicas exhibited structures with high specific surface area and pore volume and tended to have a similar pore diameter but more optimized SBA-15 structures tended to afford better ordered inverse carbon replicas. Regular and PHTS SBA-15 samples were additionally studied using argon adsorption at 77 K, which provided an important insight into the plugged structure. In particular, a PHTS sample that on the basis of nitrogen adsorption at 77 K appeared to be fully plugged, that is, with all primary mesopore channels closed by finely porous plugs, was found to be only partially plugged based on argon adsorption at 77 K, although there was evidence for the presence of some constrictions in all of the channels. A mechanism of the plug formation at high TEOS/copolymer molar ratios is proposed on the basis of similarity of the PHTSs with as-synthesized SBA-15 subjected to postsynthesis modification with TEOS. It is proposed herein that when the TEOS/EO-unit molar ratio is excessively high, only a part of TEOS present initially interacts with the EO_n blocks of the copolymer template and thus hydrolyzes and condenses faster to form the SBA-15 structure. Subsequently or concurrently, the remaining TEOS, which hydrolyzes and condenses more slowly, solubilizes in the copolymer template in the SBA-15 pores (perhaps in the poly(propylene oxide) core of the micelles), or displaces the template, and then condenses to form the plugs.

1. Introduction

In 1998, it was first reported that a silica with large, uniform mesopores arranged into a two-dimensional (2-D) hexagonal structure can readily be synthesized using triblock copolymer and oligomer templates with poly(ethylene oxide) (EO_n) blocks.[1,2] This ordered mesoporous material, denoted SBA-15, was initially thought to exhibit unconnected channel-like pores, thus being an MCM-41 analogue with very large pores, thick pore walls, and superior hydrothermal stability. However, platinum and carbon replication studies[3−5] revealed that ordered mesopores of SBA-15 are actually connected through complementary pores (micropores and small mesopores) in the siliceous pore walls. It was proposed that the formation of these connecting pores is related to the fact that EO_n blocks of the template are occluded in siliceous walls of as-synthesized SBA-15 to such an extent that the structure with connected pores is obtained after the template removal.[4,6] SBA-15 can be readily synthesized using cheap, commercially available polymers and oligomers, and it exhibits attractive structural properties, such as tailorable pore size, high degree of structural ordering, and very good hydrothermal stability.[1,2] Moreover, the synthesis of SBA-15 and similarly structured materials can be accomplished using a cheap silica source, sodium silicate,[7−9] which makes this synthesis commercially viable. Because of these desirable features, SBA-15 attracted much attention. A lot of work was devoted to the implantation of Al,[10] Ti,[11] and V[12] heteroatoms in SBA-15 framework and to the surface grafting of zirconia,[13] sulfated zirconia,[14] VO_x-SbO_x species,[15] rare earth oxides,[13,16] and iron oxide,[13] which allow one to obtain a large-pore ordered mesoporous catalysts. Catalytic properties can be also imparted by dispersing Co and Ni particles on SBA-15 support.[17,18] SBA-15 is promising for the manufacturing of waveguides, mirrorless lasers,[19] fast response photochromic mesostructures,[20] superradiant fluorescent nanomaterials,[21] and sensing devices.[22] This silica can also be used for the immobilization of enzymes,[23−26] which exhibit catalytic activity,[25,26] and for the sequestration and release of proteins.[27] After surface modification with

* To whom correspondence should be addressed. Prof. M. Jaroniec (E-mail: jaroniec@kent.edu. Phone: 330-672-3790. Fax: 330-672-3816) and Prof. R. Ryoo (E-mail: rryoo@mail.kaist.ac.kr).

[†] Kent State University.

[‡] Korea Advanced Institute of Science and Technology.

10.1021/jp0271514 CCC: $25.00
Published on Web 02/13/2003

organosilanes, SBA-15 is suitable as a packing material for HPLC separations of biomolecules,[28] and as an adsorbent for heavy metal ions,[29,30] whereas unmodified SBA-15 silica was found promising for separations of light hydrocarbons.[31] Some work on molecular imprinting of SBA-15 was also carried out.[32] Another highly promising area of applications of SBA-15 is its use as a host or template for the synthesis of nanowires and ordered inverse replicas. This includes the synthesis of (i) 2-D hexagonally ordered mesoporous Pt;[3,4] (ii) Ag,[33,34] Au,[34] Pt,[4,34] Pd,[35] Cu,[36] and Ni[36] nanowires; (iii) semiconductor nanocrystals of PbS[37] and CdS;[38] (iv) magnetic clusters;[39] (v) polypyrrole/poly(methyl methacrylate) coaxial nanocables;[40] (vi) ordered mesoporous polymer networks;[41] and (vii) ordered mesoporous carbons consistent of 2-D hexagonally ordered arrays of rods[5] or nanotubes[42] (these two types of ordered carbons are denoted CMK-3 and CMK-5 respectively). It should be noted that in many of the above cases (see ii−iv), it was assumed that nanowires and nanocrystals formed in a particular pore are separated from those in adjacent pores. However, because of the well-documented tendency to form 2-D hexagonally ordered platinum[3,4] or carbon nanostructures[5,42] in SBA-15 templates, such assumptions may be invalid and the actual form of the nanostructures formed in SBA-15 template may require further verification. SBA-15 films can also be used to direct the growth of multiwall carbon nanotubes.[43]

Very recently, it was demonstrated that when SBA-15 silica is synthesized at high TEOS: polymeric template molar ratios (TEOS stands for tetraethyl orthosilicate,), a fraction of ordered mesopores exhibits porous plugs within the mesoporous channels.[44−47] These SBA-15 silicas, referred to as plugged hexagonal templated silicas (PHTSs), were claimed to exhibit a tailorable relative amount of open and plugged pores, and in particular, all pores were reported to be plugged in some PHTSs. PHTSs were found to exhibit a remarkable mechanical stability that was much higher than that of SBA-15 silica synthesized using a typical procedure.[44−46] PHTSs also exhibited excellent hydrothermal stability and good thermal stability.[45,46] The high stability and an appreciable degree of structure tailorability make PHTSs potentially attractive as adsorbents, encapsulation media, and so forth.

The synthesis of CMK-3 and CMK-5 carbons using SBA-15 and similarly structured silicas as templates has recently attracted much attention.[5,42,48−54] This has been fueled by prospects of the application of these materials as adsorbents, catalyst supports, electrical double-layer capacitors, materials for fuel-cell technologies,[42,49] and templates for the synthesis of ordered inorganic materials.[53,54]

In this study, a series of SBA-15 silicas was synthesized using triblock copolymer templates with the same length of PO_m block ($m = 70$) but different average lengths of EO_n blocks ($n = 17-28$), which was achieved by mixing $EO_{20}PO_{70}EO_{20}$ copolymer with either $EO_5PO_{70}EO_5$ or $EO_{106}PO_{70}EO_{106}$ copolymer. Silica precursor (TEOS):copolymer molar ratios were also varied for one of these copolymer templates. The resulting regular and plugged SBA-15 silicas were successfully used to synthesize inverse carbon replicas of CMK-3 type. The obtained materials were characterized using nitrogen adsorption, and selected samples were further characterized using argon adsorption at 77 K, which provided important information about the nature of the plugs. A new mechanism for the plug formation is proposed which suggests that the formation of the plugs at high TEOS:copolymer ratios is similar in nature to the postsynthesis modification of as-synthesized SBA-15 with TEOS (reported earlier in ref 30), which was found to afford materials of adsorption properties analogous to those of PHTSs.

TABLE 1: Synthesis Mixture Composition for the SBA-15 Samples (Expressed as a Mass of Reagents in Grams)

sample	average length (n) of EO_n blocks	block copolymer $EO_nPO_{70}EO_n$ L121 ($n = 5$)	P123 ($n = 20$)	F127 ($n = 106$)	TEOS	1.6M HCl
SBA-15-A	17	0.65	3.35		7.59	150
SBA-15-B	18.5	0.32	3.68		8.05	150
SBA-15-C1	20		4		8.5	150
SBA-15-C2	20		4		12.75	150
SBA-15-C3	20		4		17	150
SBA-15-D	23		3.6	0.4	9.62	150
SBA-15-E	26		3.24	0.76	10.73	150

2. Experimental Section

2.1. Materials. SBA-15 silicas were synthesized in a similar way as that originally reported by Zhao et al.[1,2] using poly(ethylene oxide)−poly(propylene oxide)−poly(ethylene oxide) triblock copolymers $EO_nPO_{70}EO_n$ as templates. The average number of EO units in the EO_n block of the template was varied from $n = 17$ to 28, using mixtures of $EO_{20}PO_{70}EO_{20}$ (Pluronic P123) with either $EO_5PO_{70}EO_5$ (Pluronic L121, BASF) or $EO_{106}PO_{70}EO_{106}$ (Pluronic F127). The synthesis mixture compositions used are listed in Table 1. In a typical synthesis, 4.0 g of $EO_{20}PO_{70}EO_{20}$ copolymer was dissolved in 150 g of 1.6 M HCl. To this solution was added 8.50 g of TEOS, and the resulting mixture was stirred until TEOS was dissolved. The mixture was placed in an oven for 24 h at 308 K and then 24 h more at 373 K under static condition. Silica products were filtered, dried (without washing), and calcined at 823 K. The amount of TEOS was varied (see Table 1) to maintain a constant TEOS/EO-unit molar ratio for copolymer blends of different average EO_n chain length. In addition, the synthesis mixtures with different TEOS/EO-unit molar ratios were used for $n = 20$; that is, the TEOS/$EO_{20}PO_{70}EO_{20}$ molar ratio was varied from 59 to 118. The SBA-15 samples are denoted SBA-15-X or SBA-15-Xy, where X is A, B, C, D, and E for $n = 17$, 18.5, 20, 24, and 28, respectively, and y is 1, 2, or 3 for TEOS/copolymer molar ratios of 59 (which corresponds to the same TEOS/EO-unit molar ratio as that for samples A, B, D and E), 89, and 118, respectively. The SBA-15 silica samples were used to synthesize inverse carbon replicas using the method reported elsewhere.[5] Briefly, the calcined silicas were infiltrated twice with sucrose solution containing sulfuric acid catalyst. The carbonization was carried out with heating to 1173 K under vacuum. The carbon−silica composites thus obtained were washed with hydrofluoric acid at room temperature, giving carbon samples. CMK-3 carbon templated by particular SBA-15-Xy silicas are denoted CMK-3-Xy. Properties of samples SBA-15-C1 and CMK-3-C1 were discussed in some detail elsewhere.[48]

2.2. Measurements. Powder X-ray diffraction (XRD) patterns were acquired on a Rigaku D/MAX-III diffractometer using Cu Kα radiation. Nitrogen and argon adsorption isotherms were measured at 77 K on a Micromeritics ASAP 2010 volumetric adsorption analyzer. The experimentally measured saturation vapor pressure for gas−solid equilibrium at 77 K was used to assess the relative pressure in argon adsorption measurements. Before the adsorption measurements, samples were outgassed under vacuum for 2 h at 473 K in the port of the adsorption analyzer.

2.3. Calculations. Because of the fact that the diffractometer used did not provide accurate values of positions of peaks on

XRD patterns at very low angles where (100) peak was observed, the unit-cell parameter, *a*, for 2-D hexagonal structure was calculated from the positions of (110) and (200) peaks, if these peaks were distinct. Otherwise, the unit-cell parameter was calculated from the position of the (100) peak. The BET specific surface area[55] was calculated from adsorption data in the relative pressure interval from 0.04 to 0.2. Cross-sectional areas of 0.162 and 0.138 nm^2 were used for the nitrogen molecule and argon atom, respectively, in the BET calculations. The total pore volume[55] was estimated from the amount adsorbed at a relative pressure of 0.99. In these and other pore volume calculations from argon adsorption data, it was assumed that argon condensed in pores at 77 K exhibits the same density as bulk liquid argon at 87 K, that is, 1.400 g cm^{-3}.[56,57] The micropore volume of SBA-15 silicas was estimated from nitrogen adsorption data using the α_s plot method[6,55,58] in the α_s range from 0.9 to 1.2.[6] It should be noted that α_s is the standard reduced adsorption defined as a ratio of amount adsorbed for the reference adsorbent at a given relative pressure to the amount adsorbed at a relative pressure of 0.4.[55,58] The external surface area and the sum of the primary (ordered) mesopore volume and micropore volume for the SBA-15 silicas were evaluated from data in the α_s range from 1.75 to 2.2 (except for the SBA-15-B sample, for which an interval from 1.8 to 2.2 was used). The reference nitrogen adsorption isotherm data for macroporous silica[58] were used in these α_s plot calculations. In the case of CMK-3 carbons, the external surface area and the sum of the primary mesopore volume and micropore volume (including the volume of mesopores that can be regarded as defects in the CMK-3 structure) were evaluated from nitrogen adsorption data using the α_s plot method in the α_s interval from 1.8 to 2.2.[51] The reference nitrogen adsorption isotherm data for a macroporous carbon black[59] were used in the α_s plot calculations for the CMK-3 carbons. The pore size distributions (PSDs) were calculated from nitrogen and argon adsorption data using an algorithm based on ideas of Barrett, Joyner, and Halenda (BJH)[60] (without simplifying assumptions proposed by these authors). In these calculations, the employed relations between the capillary condensation pressure and the pore diameter for cylindrical pores were derived using model ordered mesoporous materials (mostly MCM-41 silicas) as proposed by Kruk, Jaroniec, and Sayari (KJS).[56,61] The maximum on the KJS PSD is considered as the primary mesopore diameter for a given sample. For SBA-15 silicas, the primary mesopore diameter, w_d, was additionally evaluated using a geometrical equation derived for a material with 2-D hexagonally ordered pores and with microporosity in the pore walls:[9,62]

$$w_d = 1.05\, a\left(\frac{V_p}{1/\rho + V_p + V_{mi}}\right)^{0.5} \qquad (1)$$

where a is the unit-cell parameter, V_p is the primary mesopore volume, V_{mi} is the micropore volume, and ρ is pore wall density assumed to be equal to that of amorphous silica (2.2 g cm^{-3}). It should be noted that the micropore volume assessed using the α_s plot method for SBA-15 may be underestimated,[63] which would result in the pore size overestimation using eq 1.

3. Results and Discussion

3.1. SBA-15 Silicas. *XRD.* As can be seen in Figure 1, powder XRD patterns for the silicas obtained using the five triblock copolymer templates exhibited three peaks that can be indexed on a 2-D hexagonal lattice, and thus, these materials can be regarded as SBA-15 silicas.[1,2] This is consistent with earlier results, which suggested that in the case of $EO_nPO_mEO_n$ copolymers, 2-D hexagonal structure (SBA-15) forms when the ratio of the number of EO blocks to the number of PO blocks (2n/m) is between 0.07 and 1.5.[64] In our case, this ratio was in the range from 0.49 to 0.8, which is within the aforementioned interval. Another study also reported formation of the SBA-15 structure for templates with an appreciable range of lengths of the EO_n blocks, when the size of the PO_m block was kept approximately constant.[65] The XRD patterns were better resolved for intermediate length of the EO_n block (samples SBA-15-B, -C1, and -D for which $n = 18.5$, 20, and 24). The increase in the TEOS/EO-block molar ratio (SBA-15-C1, -2, and -3) led to some loss of resolution of the XRD patterns. The unit-cell parameters for the calcined SBA-15 samples (see Table 2) were similar to those reported in the literature for the copolymeric templates of a similar size.[1,2,6] For samples synthesized with the same TEOS/EO-block molar ratio, the largest unit-cell sizes were recorded for medium EO_n block lengths ($n = 18.5$, 20, and 24). For the $EO_{20}PO_{70}EO_{20}$ template, the unit-cell size of the calcined SBA-15 was found to decrease as the TEOS/copolymer ratio increased, similarly to results reported earlier.[44−46]

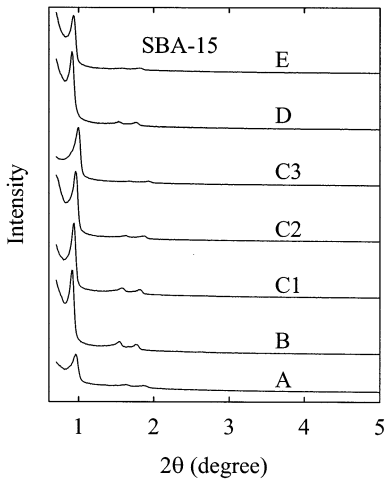

Figure 1. Powder XRD patterns for the SBA-15 silicas.

Nitrogen Adsorption. Nitrogen adsorption isotherms for the SBA-15 samples are shown in Figure 2, whereas structural parameters determined on the basis of these isotherms are listed in Table 2. It can be seen that for the constant TEOS/EO-unit ratio, the adsorption capacity, BET specific surface area, primary (ordered) mesopore volume, and pore diameter (see PSDs in Figure 3) reached their maximum for $n = 18.5$ (sample SBA-15-B). The BET specific surface areas were in the range from 670 to 900 $m^2\ g^{-1}$, primary mesopore volumes were from 0.51 to 0.98 $cm^3\ g^{-1}$, and the pore diameters were from 8.3 to 9.5 nm. All of these samples exhibited adsorption isotherms typical for SBA-15 silicas,[1,6] that is, with relatively narrow hysteresis loops of H1 type.[55] On the other hand, the increase in the TEOS/EO-unit molar ratio in the synthesis mixture not only led to a decreased specific surface area (from 850 to 790 $m^2\ g^{-1}$), primary mesopore volume (from 0.86 to 0.58 $cm^3\ g^{-1}$), and pore diameter (from 9.0 to 7.2 nm, see PSDs in Figure 4) but also resulted in an appreciable widening and/or tailing of hysteresis loops. Van Der Voort et al. have already reported SBA-15 silicas with similar adsorption properties,[44−46] and they attributed these properties to the formation of porous plugs in the ordered channels of SBA-15 for higher TEOS/copolymer ratios. These authors claimed[45] that their sample PHTS-3 with nitrogen adsorption isotherm similar to our SBA-15-C3 sample did not exhibit any open (that is, not plugged) pores, whereas

TABLE 2: Structural Properties of the SBA-15 Silicas Determined from Nitrogen Adsorption and XRD Data[a]

sample	a (nm)	S_{BET} (m^2 g^{-1})	V_t (cm^3 g^{-1})	V_p (cm^3 g^{-1})	V_{mi} (cm^3 g^{-1})	S_{ex} (m^2 g^{-1})	w_{KJS} (nm)	w_d (nm)
SBA-15-A	10.9	670	0.76	0.51	0.08	100	8.8	8.0
SBA-15-B	11.5	900	1.16	0.98	0.08	70	9.5	9.7
SBA-15-C1	11.2	850	1.03	0.86	0.08	60	9.0	9.2
SBA-15-C2	10.9	810	0.83	0.68	0.11	20	7.9	8.4
SBA-15-C3	10.6	790	0.71	0.58	0.11	10	7.2	7.9
SBA-15-D	11.5	870	0.95	0.76	0.13	40	8.8	9.1
SBA-15-E	11.2	900	0.89	0.72	0.14	20	8.3	8.7

[a] Notation: a, unit-cell parameter determined from XRD (110) and (200) interplanar spacings; S_{BET}, BET specific surface area; V_t, total pore volume; V_p, primary mesopore volume; V_{mi}, micropore volume; S_{ex}, external surface area; w_{KJS}, pore diameter evaluated using the KJS method; w_d, pore diameter evaluated from geometrical considerations (eq 1).

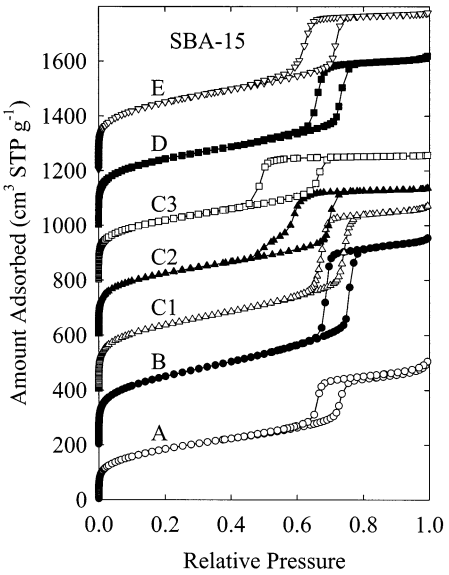

Figure 2. Nitrogen adsorption isotherms for the SBA-15 silicas. The isotherms for samples B, C1, C2, C3, D, and E were offset vertically by 200, 400, 600, 800, 1000, and 1200 cm^3 STP g^{-1}, respectively.

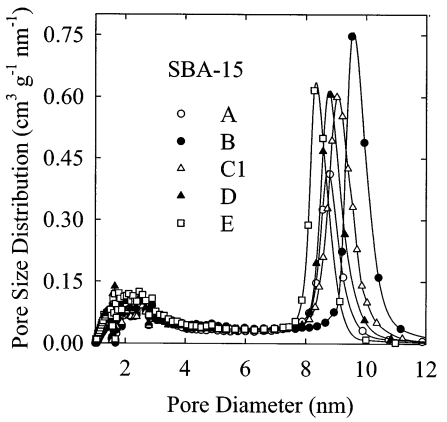

Figure 3. Pore size distributions calculated from nitrogen adsorption data at 77 K for the SBA-15 silicas synthesized with a typical TEOS/EO-unit molar ratio.

the material PHTS-2, whose nitrogen adsorption isotherm was quite similar to that for our SBA-15-C2 sample, had fractions of both open and plugged pores. As it is shown below on the basis of argon adsorption data measured at 77 K,[56,66] this interpretation is speculative and may be incorrect.

As expected for SBA-15 silicas, all samples were appreciably microporous[4,6] (see PSDs in Figures 3 and 4, and micropore volumes listed in Table 1). Interestingly enough, the micropore volume tended to increase as the length of the EO_n block increased (at constant TEOS/EO-unit ratio), which is expected from the fact that the micropores in SBA-15 originate from

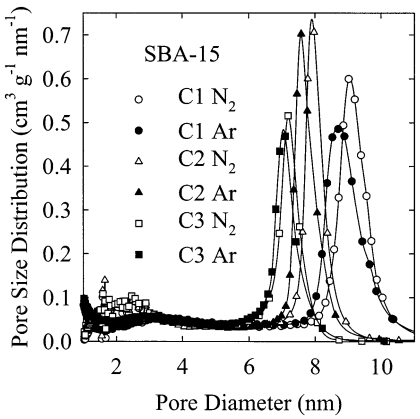

Figure 4. Pore size distributions calculated from nitrogen and argon adsorption data at 77 K for the SBA-15 silicas synthesized with different TEOS/EO-unit molar ratios.

spaces in the silica matrix, where EO_n chains of the template were located.[4,6] Consistent with results reported earlier,[44−46] the plugged SBA-15-C2 and -C3 samples exhibited increased microporosity. All of the samples exhibited rather low external surface areas (70 m^2 g^{-1} or lower), except for the SBA-15-A sample that exhibited a more pronounced secondary mesoporosity and the external surface area of about 100 m^2 g^{-1}. It is also interesting to note that the maxima on the KJS PSDs were close to the pore diameters assessed using the geometrical equation (eq 1), especially for SBA-15 samples that were not plugged.

Argon Adsorption. Additional insight into the structures of the plugged SBA-15 silicas was obtained from argon adsorption data acquired at 77 K. These conditions are favorable for studies of materials with constrictions in porous structures, because of the nature of the adsorption−desorption process in pores with constrictions. Namely, in the case of a pore that is connected with the neighboring pores or with the surroundings through entrances (constrictions) of diameter smaller than the diameter of the pore, capillary evaporation from the pore interior is delayed until the capillary evaporation from the constrictions takes place (unless the lower limit of adsorption−desorption hysteresis is reached, see below).[55,61,67−69] This behavior is often referred to as a pore blocking phenomenon affecting the position of the desorption branch of the hysteresis loop and is typically associated with adsorption−desorption in ink-bottle pores. In this case, the diameter of the constrictions can be related to the position of the desorption branch of the isotherm. However, this mechanism of capillary evaporation is operative only above the lower pressure limit of adsorption−desorption hysteresis.[67−69] When this limit is reached, the capillary evaporation from the wide pore interior can no longer be delayed by the adsorbate condensed in the constrictions and the capillary evaporation from the pore interior takes place at the pressure corresponding to

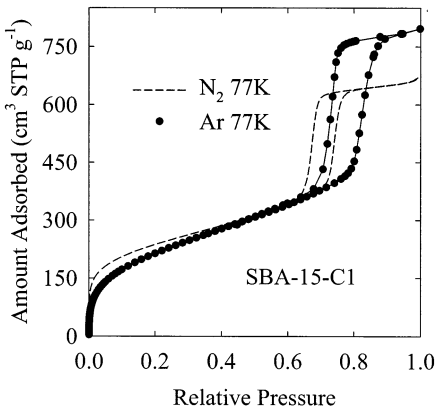

Figure 5. Comparison of nitrogen and argon adsorption isotherms for the SBA-15 silica synthesized with a typical TEOS/EO-unit molar ratio.

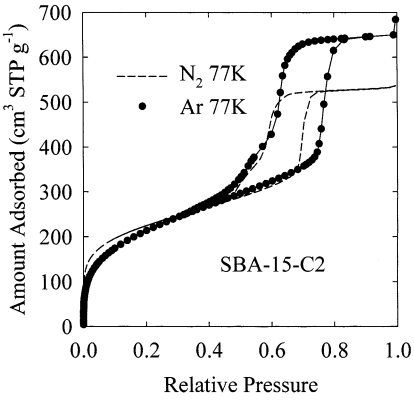

Figure 6. Comparison of nitrogen and argon adsorption isotherms for the plugged SBA-15 silica synthesized with a higher TEOS/EO-unit molar ratio.

the lower limit of hysteresis.[61,67−69] In this case, the position of the desorption branch is not related to the size of the constrictions.[68] Therefore, in studies of the size of constrictions on the basis of desorption branches of isotherms, it is beneficial to use conditions, in which adsorption−desorption hysteresis is observed in as wide range of pore sizes as possible.[66] From this point of view, argon adsorption at 77 K is superior from nitrogen adsorption at 77 K,[66] because in the former case, the lower limit of adsorption−desorption hysteresis (relative pressure range ∼0.27−0.38) coincides with capillary evaporation from pores ∼3.4−4.0 nm in diameter (see ref 56), compared to ∼4.0−5.0 nm for nitrogen at 77 K (lower limit at a relative pressure of ∼0.40−0.50). This allows one to use argon at 77 K to probe a wider range of diameters of constrictions in the porous structure (down to ∼4 nm vs ∼5 nm in the case of nitrogen) simply by analyzing the shape of the desorption branch of the isotherm and, thus, to gain additional insight into the existence of constrictions of sizes in the range from about 4 to 5 nm.[66] To illustrate advantages of argon adsorption at 77 K in probing porous structures with constrictions, let us consider nitrogen and argon adsorption at 77 K for samples SBA-15-C1, -C2, and -C3. In the case of sample -C1, both argon and nitrogen isotherms exhibited hysteresis loops of H1 type, that is, narrow and with approximately parallel branches (see Figure 5). On the other hand, the hysteresis loops on adsorption isotherms for the SBA-15-C2 sample (Figure 6) were somewhat broader and exhibited some tailing. In the case of nitrogen adsorption, the tail ended more abruptly at a relative pressure somewhere between 0.45 and 0.5, which corresponds to a lower limit of adsorption−desorption hysteresis. The broadening observed on

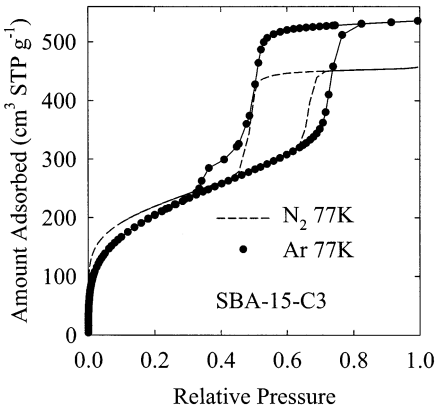

Figure 7. Comparison of nitrogen and argon adsorption isotherms for the plugged SBA-15 silica synthesized with the highest TEOS/EO-unit molar ratio.

the hysteresis loops can be attributed to the decrease in the uniformity of diameter along the pore channels,[61] which may be related to the increase in the degree of surface corrugation or to the development of constrictions in the porous structure. The tailing is likely to be related to the second of these factors. In the case of argon adsorption at 77 K for the SBA-15-C2 sample, the tail of the hysteresis loop appeared to reach its closure (ending) point essentially before the lower limit of adsorption−desorption hysteresis was reached. Such a behavior indicates that essentially all constrictions in the porous structure of this material are likely to exhibit diameters above ∼4 nm.

Argon adsorption at 77 K was particularly revealing in the case of the SBA-15-C3 sample, for which the hysteresis loop on its nitrogen isotherm was quite broad (see Figure 7 and compare it with Figure 5) and closed quite abruptly in the proximity of the lower limit of adsorption−desorption hysteresis. This indicates that the constrictions in the pore structure are primarily below ∼5 nm in diameter. In the case of argon adsorption at 77 K, the hysteresis loop was also broad, but the rapid decline of the desorption branch at relative pressures between 0.46 and 0.53 was followed by tailing (somewhat similar to that observed for SBA-15-C2) which extended down to the lower limit of adsorption−desorption hysteresis. This shows that the extent of plugging for samples SBA-15-C2 and -C3 was quite similar, although the variations in the pore diameter along the channels were higher (as inferred from larger width of the hysteresis loops) and the diameter of pores in the plugs was lower for the latter. Only for the SBA-15-C3 sample, there is an appreciable fraction of constrictions of diameter below about 4.0 nm, whose size is impossible to estimate from the shape of the desorption branch of the hysteresis loop for argon and nitrogen at 77 K. It should be noted that Van der Voort et al.[44] claimed that their PTHS-3 sample, for which the nitrogen adsorption isotherm was similar to that for SBA-15-C3, did not exhibit any open (not plugged) mesopores. On the basis of our argon adsorption data for SBA-15-C3, this claim is rather unlikely, and it appears to be more likely that only some of the pores were indeed plugged, whereas others might merely have exhibited an appreciable surface corrugation (perhaps related to incomplete plug formation), leading to the observed broadening of the hysteresis loop. Our results demonstrate that nitrogen adsorption is not a preferable method to elucidate the plug formation in SBA-15, and argon adsorption at 77 K may be much more informative. Unfortunately, the latter method can probe size and connectivity of pores of diameter not larger than about 15 nm,[56] because argon does not exhibit capillary condensation is wider pores. Finally, it should be noted

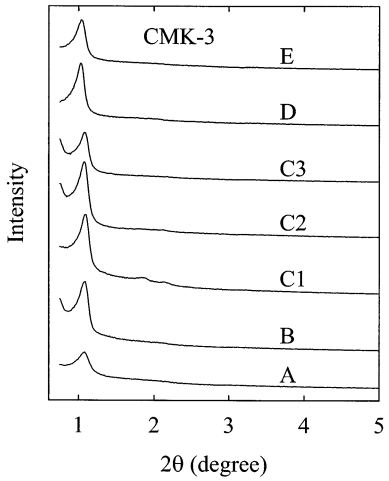

Figure 8. Powder XRD patterns for the carbon inverse replicas (ordered mesoporous carbons of CMK-3 type) synthesized using the SBA-15 silica templates.

that plugs with pores of sizes within or close to the micropore range can be characterized using a method based on the monitoring of results of the modification with surface groups of different sizes.[70] This procedure would be particularly useful for essentially fully plugged samples (based on argon adsorption at 77 K and assuming that such materials can be obtained), and in such a case, it is likely to allow one to approximately map out the size distribution of the pores in the plugs.

PSD and pore volume estimates for the SBA-15-C1, -C2, and -C3 silicas based on argon adsorption data were similar to those based on nitrogen adsorption data (see for instance PSDs in Figure 4). However, in comparison to nitrogen BET specific surface areas (Table 2), argon adsorption provided lower estimates of the BET specific surface area (680, 680, and 650 $m^2\ g^{-1}$, for samples SBA-15-C1, -C2, and -C3, respectively). This is a typical result and the specific surface areas for silicas evaluated from argon data in a way employed here are likely to be more accurate than the nitrogen BET surface areas.[56,57]

3.2. SBA-15/Carbon Composites. The composites exhibited single pronounced peaks on their XRD patterns. They were essentially microporous and exhibited the BET specific surface areas of 330−430 $m^2\ g^{-1}$ and total pore volumes of 0.16−0.20 $cm^3\ g^{-1}$. No evidence of accessible ordered mesoporosity was found, which suggests that the infiltration of the ordered mesopores of the silica template with the carbon precursor was uniform.

3.3. CMK-3 Carbons. *XRD.* Powder XRD patterns for the CMK-3 carbons featured at least one clear XRD peak (see Figure 8), whose position corresponded to the unit-cell size somewhat smaller (by 11−17%) from that for the corresponding SBA-15 silica template (see Tables 2 and 3). The XRD patterns for the CMK-3 carbons were somewhat less well resolved than those for the corresponding SBA-15 silicas (see Figures 1 and 8), but interestingly enough, the replication did not change a relation between the intensity of the main XRD peak among the samples. For instance, the SBA-15-A template that exhibited the least intense (100) peak among the SBA-15 samples gave rise to the CMK-3-A inverse replica, which exhibited the least intense (100) peak among the CMK-3 carbons. In all cases, the (100) peak of the replica was appreciably broader than that of the corresponding template. The formation of the ordered inverse replicas for all of the SBA-15 samples considered here provided an additional confirmation of our earlier contention that the connectivity of the ordered mesopores of SBA-15 is related to the inherent properties of the templates with EO_n blocks and thus is not likely to depend on the details of the structure of the particular template and on the synthesis conditions.[4,6]

TABLE 3: Structural Properties of the CMK-3 Carbons Determined from Nitrogen Adsorption and XRD Data[a]

sample	a (nm)	S_{BET} ($m^2\ g^{-1}$)	V_t ($cm^3\ g^{-1}$)	$V_p + V_{mi}$ ($cm^3\ g^{-1}$)	S_{ex} ($m^2\ g^{-1}$)	w_{KJS} (nm)
CMK-3-A	9.5[b]	1400	1.11	0.97[c,d]	90[d]	4.4
CMK-3-B	9.6	1640	1.32	1.24	40	4.2
CMK-3-C1	9.6	1160	1.24	1.10[c,d]	100[d]	5.7
CMK-3-C2	9.7	1280	1.09	1.02	40	4.7
CMK-3-C3	9.4[b]	1250	1.09	1.01	40	4.8
CMK-3-D	10.1	1530	1.28	1.20	40	4.5
CMK-3-E	9.8[b]	1430	1.12	1.07	30	4.4

[a] Notation: see Table 2. [b] Unit-cell parameter calculations were based on the position of (100) XRD peak, which may be inaccurate (the unit-cell parameter may be underestimated). The (110) and (200) peaks were not distinct on the XRD patterns. [c] Includes the volume of pores that can be regarded as defects in ordered mesoporous structure. [d] This estimate may be inaccurate because of the lack of sufficiently broad interval of α_s values suitable for the calculations.

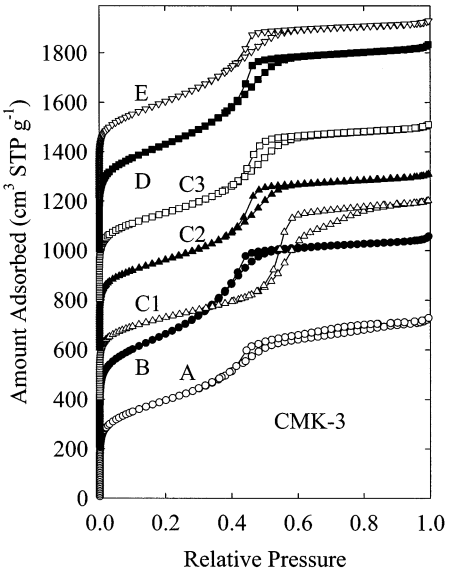

Figure 9. Nitrogen adsorption isotherms for the CMK-3 ordered mesoporous carbons synthesized using the SBA-15 silica templates. The isotherms for samples B, C1, C2, C3, D, and E were offset vertically by 200, 400, 600, 800, 1000, and 1200 cm^3 STP g^{-1}, respectively.

Nitrogen Adsorption. As determined from nitrogen adsorption data (Figure 9), all of the inverse carbon replicas were high-surface-area (S_{BET} = 1160−1640 $m^2\ g^{-1}$, see Table 3), large-pore-volume (V_t = 1.09−1.32 $cm^3\ g^{-1}$) materials. CMK-3 carbons synthesized in a way employed here are known to exhibit microporous carbon frameworks,[5] and the microporosity partially accounts for the large BET specific surface areas of these materials. The nitrogen adsorption isotherms for all of the carbons were generally similar, featuring steps of capillary condensation in primary mesopores at relative pressures somewhere between 0.35 and 0.55, although the step for the CMK-3-C1 sample was located at somewhat higher pressure. Samples -A and -C1 also exhibited a noticeable increase in adsorption after the completion of the capillary condensation in primary mesopores, which indicated the presence of appreciable secondary mesoporosity. In the case of the CMK-3-A sample, this secondary porosity primarily arises from the replication of the secondary porosity of the SBA-15-A template, but in the case of the CMK-3-C1 sample, the occurrence of secondary porosity

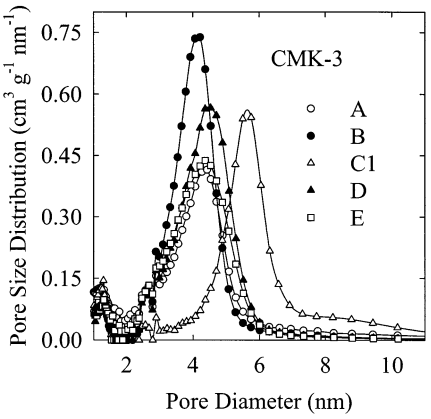

Figure 10. Pore size distributions calculated from nitrogen adsorption data at 77 K for the CMK-3 carbons synthesized using the SBA-15 silica templates obtained with a typical TEOS/EO-unit molar ratio.

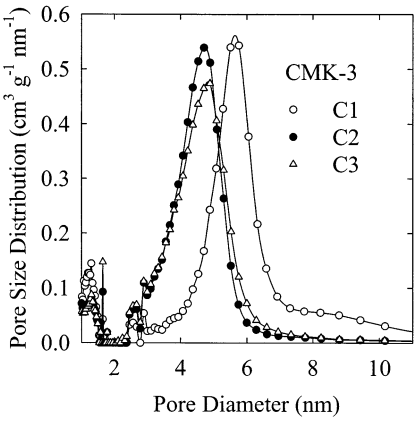

Figure 11. Pore size distributions calculated from nitrogen adsorption data at 77 K for the CMK-3 carbons synthesized using the SBA-15 silica templates obtained with different TEOS/EO-unit molar ratios.

points to the existence of defects in the ordered carbon structure.[51] All CMK-3 carbons exhibited a very similar primary mesopore diameter of about 4.5 nm, except for the CMK-3-C1 sample, whose pore diameter was larger by about 1 nm (see Table 3 and PSDs in Figures 10 and 11). The reason why this sample exhibited such peculiar properties is not clear. In general, SBA-15 silicas with larger adsorption capacities (as seen from adsorption) and better structural ordering (as seen from XRD) tended to afford CMK-3 carbons with higher peaks on PSDs, and thus with higher primary mesopore volumes.

3.4. Explanation of the Formation of Plugs in SBA-15 Silicas Synthesized at High TEOS/Copolymer Ratios. Van Der Voort et al.[44−46] related the formation of the plugs to the presence of impurities, such as diblock copolymers and block polymers, in the triblock copolymer template. They stipulated that these impurities may not act as templates in the formation of ordered mesopores, but may be capable of templating "the disordered nanocapsules, including a complementary porosity".[44,45] It is known that poly(ethylene) blocks can indeed interact with silica precursors, giving rise to the formation of disordered, usually microporous silicas.[71] Moreover, it is reasonable to assume that when the TEOS/copolymer ratio is increased there might be a tendency for the silica precursors to interact with polymeric species that are perhaps less suitable as templates or weakly interacting with the silica precursors. However, it is known that polymer templates can be readily mixed, which results in the formation of a templated silica of a single structure, rather than a mixture of silicas templated by different components of the mixture (see refs 64, 72, 73, and results reported herein) Moreover, PO_n polymers can be used as expanders in the SBA-15 silica formation, which suggests their facile solubilization in the micelles formed by triblock copolymers.[74,75] This would suggest that any impurities, such as diblock copolymers or single block polymers, are likely to be included in the micelles of the triblock copolymer and thus not available as templates for the plug formation.

Herein, a different mechanism of the formation of the plugs is proposed. First, one can notice that silicas similar to the PHTSs synthesized at high TEOS/copolymer ratio were reported to form when as-synthesized (polymer-containing) SBA-15 was reacted with TEOS and subsequently calcined.[30] In this case, hysteresis loops with characteristic tailing were also observed, and even adsorption capacities of these TEOS-modified materials were similar to those of PHTSs. Therefore, it is proposed that the formation of plugs is a result to a secondary process of the reaction of excess TEOS with the preformed copolymer-templated SBA-15 structure. Such a scenario is certainly possible because the presence of the surfactant template (whether cationic, or oligomeric) has been reported to facilitate the hydrolysis and/or condensation of silica species.[76−80] However, the capability of the template to facilitate these two processes is likely to be related with the accessibility of the template for the silica species. If the amount of the silica precursor (TEOS) is too high with respect to the amount of the template, some amount of the silica precursor may have no access to the EO_n blocks of the template (these blocks have been suggested to facilitate the hydrolysis and condensation of TEOS)[79] and may not hydrolyze/condense at an accelerated rate. Subsequently, unhydrolyzed or partially hydrolyzed excess TEOS can solubilize in copolymer micelles contained in the already-formed silica structure of as-synthesized SBA-15, and finally, the excess TEOS can functionalize the silica surface, forming irregular silica deposits. This would lead to the plug formation in a way analogous to that in the postsynthesis functionalization.[30] Another possible mechanism can also be envisioned. In the case where an excess of TEOS is used, a part of TEOS can interact with EO_n chains of the template and undergo accelerated hydrolysis and condensation, whereas an excess amount of TEOS can be partially or completely solubilized in the PO_m micellar core, wherein the hydrolysis and condensation of silica species is retarded. This solubilized excess TEOS would then slowly undergo hydrolysis and condensation, thus leading to the formation of the plugs, as described above.

Van Der Voort et al.[81] suggested that the plugs can form at high TEOS/copolymer ratios in the case of the synthesis of not only SBA-15 but also SBA-16. The mechanism of the plug formation proposed herein leads to the same conclusion, and in more general terms, it provides the basis of a prediction that plugs may form in all cases of polymer or oligomer templated silica synthesis, where TEOS is used in an excessive amount.

4. Conclusions

Triblock copolymers of $EO_nPO_{70}EO_n$ type (or mixtures thereof) with average n in the range from 17 to 28 readily template the formation of SBA-15 silicas. An optimal length of the EO_n block is about 19 in the conditions studied herein. The interconnected nature of ordered pores of these SBA-15 silicas was confirmed by using the carbon inverse replication technique to synthesize ordered mesoporous carbons of CMK-3 type. The formation of constrictions and plugs in the primary mesopores was observed for higher TEOS/copolymer ratios in the synthesis mixture, as expected from the results recently

published by Van Der Voort et al. The existence of the plugs did not appear to have any noticeable impact on XRD and adsorption properties of the carbon inverse replicas, whose successful synthesis using PHTS templates has been demonstrated here for the first time. In studies of porous structures of plugged SBA-15 silicas, argon adsorption at 77 K tends to be more informative than nitrogen adsorption, allowing to distinguish more clearly between pores with constrictions or corrugated surface and pores with plugs. In favorable cases, argon adsorption may also allow one to elucidate better the diameter of constrictions or pores in the plugs. A new mechanism of formation of the plugs is proposed, which explains an earlier finding that plugged SBA-15 materials form not only at high TEOS/copolymer ratio in the direct synthesis but also in the case of postsynthesis modification of as-synthesized SBA-15 with TEOS. According to the proposed mechanism, in synthesis conditions where excess TEOS is present, only a fraction of TEOS is capable of interacting with EO_n blocks of the copolymer template and exhibits enhanced hydrolysis and condensation rates. This part of TEOS forms an ordered silica framework templated by the copolymer, whereas excess TEOS that does not interact with the template hydrolyses and condenses much more slowly. Because of that, this excess TEOS can penetrate the micellar structure of as-synthesized SBA-15 in a similar manner as in the case of the postsynthesis modification with TEOS. There is also a possibility that a certain amount of the excess TEOS can solubilize in PO_m blocks of the template (where its hydrolysis and condensation is retarded) at the beginning of the self-assembly process. This excess TEOS would hydrolyze and condense primarily after the ordered silica structure has already been assembled, forming the plugs or constrictions.

Acknowledgment. M.J. acknowledges support by NSF Grant CHE-0093707. The donors of the Petroleum Research Fund administered by the American Chemical Society are also gratefully acknowledged for a partial support of this research. R.R. acknowledges support in part by the Ministry of Science and Technology through Creative Research Initiative Program, and by School of Molecular Science through Brain Korea 21 Project.

References and Notes

(1) Zhao, D.; Feng, J.; Huo, Q.; Melosh, N.; Fredrickson, G. H.; Chmelka, B. F.; Stucky, G. D. *Science* **1998**, *279*, 548.
(2) Zhao, D.; Huo, Q.; Feng, J.; Chmelka, B. F.; Stucky, G. D. *J. Am. Chem. Soc.* **1998**, *120*, 6024.
(3) Shin, H. J.; Ko, C. H.; Ryoo, R. *J. Mater. Chem.* **2001**, *11*, 260.
(4) Ryoo, R.; Ko, C. H.; Kruk, M.; Antochshuk, V.; Jaroniec, M. *J. Phys. Chem. B* **2000**, *104*, 11465.
(5) Jun, S.; Joo, S. H.; Ryoo, R.; Kruk, M.; Jaroniec, M.; Liu, Z.; Ohsuna, T.; Terasaki, O. *J. Am. Chem. Soc.* **2000**, *122*, 10712.
(6) Kruk, M.; Jaroniec, M.; Ko, C. H.; Ryoo, R. *Chem. Mater.* **2000**, *12*, 1961.
(7) Kim, J. M.; Stucky, G. D. *Chem. Commun.* **2000**, 1159.
(8) Kim, S.-S.; Pauly, T. R.; Pinnavaia, T. J. *Chem. Commun.* **2000**, 1661.
(9) Kim, S. S.; Karkamkar, A.; Pinnavaia, T. J.; Kruk, M.; Jaroniec, M. *J. Phys. Chem. B* **2001**, *105*, 7663.
(10) Cheng, M.; Wang, Z.; Sakurai, K.; Kumata, F.; Saito, T.; Komatsu, T.; Yashima, T. *Chem. Lett.* **1999**, 131.
(11) Luan, Z.; Maes, E. M.; van der Heide, P. A. W.; Zhao, D.; Czernuszewicz, R. S.; Kevan, L. *Chem. Mater.* **1999**, *11*, 3680.
(12) Luan, Z.; Bae, J. Y.; Kevan, L. *Chem. Mater.* **2000**, *12*, 3202.
(13) Schuth, F.; Wingen, A.; Sauer, J. *Microporous Mesoporous Mater.* **2001**, *44*−*45*, 465.
(14) Hua, W.; Yue, Y.; Gao, Z. *J. Mol. Catal. A: Chem.* **2001**, *170*, 195.
(15) Zhu, K.; Ma, Z.; Zou, Y.; Zhou, W.; Chen, T.; He, H. *Chem. Commun.* **2001**, 2552.
(16) Sauer, J.; Marlow, F.; Spliethoff, B.; Schuth, F. *Chem. Mater.* **2002**, *14*, 217.
(17) Kim, S.-W.; Son, S. U.; Lee, S. I.; Hyeon, T.; Chung, Y. K. *J. Am. Chem. Soc.* **2000**, *122*, 1550.
(18) Cho, Y. S.; Park, J. C.; Lee, B.; Kim, Y.; Yi, J. *Catal. Lett.* **2002**, *81*, 89.
(19) Yang, P.; Wirnsberger, G.; Huang, H. C.; Cordero, S. R.; McGehee, M. D.; Scott, B.; Deng, T.; Whitesides, G. M.; Chmelka, B. F.; Buratto, S. K.; Stucky, G. D. *Science* **2000**, *287*, 465.
(20) Wirnsberger, G.; Scott, B.; Chmelka, B. F.; Stucky, G. D. *Adv. Mater.* **2000**, *12*, 1450.
(21) Xu, W.; Akins, D. L. *J. Phys. Chem. B* **2002**, *106*, 1991.
(22) Zhou, H.-S.; Yamada, T.; Asai, K.; Honma, I.; Uchida, H.; Katsube, T. *Stud. Surf. Sci. Catal.* **2002**, *141*, 623.
(23) Washmon-Kriel, L.; Jimenez, V. L.; Balkus, K. J., Jr. *J. Mol. Catal. B: Enzymatic* **2000**, *10*, 453.
(24) Yiu, H. H. P.; Wright, P. A.; Botting, N. P. *Microporous Mesoporous Mater.* **2001**, *44*−*45*, 763.
(25) Takahashi, H.; Li, B.; Sasaki, T.; Miyazaki, C.; Kajino, T.; Inagaki, S. *Microporous Mesoporous Mater.* **2001**, *44*−*45*, 755.
(26) Han, Y.-J.; Watson, J. T.; Stucky, G. D.; Butler, A. *J. Mol. Catal. B: Enzymatic* **2002**, *17*, 1.
(27) Han, Y.-J.; Stucky, G. D.; Butler, A. *J. Am. Chem. Soc.* **1999**, *121*, 9897.
(28) Zhao, J.; Gao, F.; Fu, Y.; Jin, W.; Yang, P.; Zhao, D. *Chem. Commun.* **2002**, 752.
(29) Liu, A. M.; Hidajat, K.; Kawi, S.; Zhao, D. Y. *Chem. Commun.* **2000**, 1145.
(30) Antochshuk, V.; Jaroniec, M.; Joo, S. H.; Ryoo, R. *Stud. Surf. Sci. Catal.* **2002**, *141*, 607.
(31) Newalkar, B.; Choudary, N. V.; Kumar, P.; Komarneni, S.; Bhat, T. S. G. *Chem. Mater.* **2002**, *14*, 304.
(32) Coutinho, D.; Acevedo, A. O.; Dieckmann, G. R.; Balkus, K. J., Jr. *Microporous Mesoporous Mater.* **2002**, *54*, 249.
(33) Huang, M. H.; Choudrey, A.; Yang, P. *Chem. Commun.* **2000**, 1063.
(34) Han, Y.-J.; Kim, J. M.; Stucky, G. D. *Chem. Mater.* **2000**, *12*, 2068.
(35) Kang, H.; Jun, Y.-w.; Park, J.-I.; Lee, K.-B.; Cheon, J. *Chem. Mater.* **2000**, *12*, 3530.
(36) Zhang, Z.; Dai, S.; Blom, D. A.; Shen, J. *Chem. Mater.* **2002**, *14*, 965.
(37) Gao, F.; Lu, Q.; Liu, X.; Yan, Y.; Zhao, D. *Nano Lett.* **2001**, *1*, 743.
(38) Gao, F.; Lu, Q.; Zhao, D. *Chem. Phys. Lett.* **2002**, *360*, 585.
(39) Coradin, T.; Larionova, J.; Smith, A. A.; Rogez, G.; Clerac, R.; Guerin, C.; Blondin, G.; Winpenny, R. E. P.; Sanchez, C.; Mallah, T. *Adv. Mater.* **2002**, *14*, 896.
(40) Jang, J.; Lim, B.; Lee, J.; Hyeon, T. *Chem. Commun.* **2001**, 83.
(41) Lim, J. Y.; Yoon, S. B.; Kooli, F.; Yu, J.-S. *J. Mater. Chem.* **2001**, *11*, 2912.
(42) Joo, S. H.; Choi, S. J.; Oh, I.; Kwak, J.; Liu, Z.; Terasaki, O.; Ryoo, R. *Nature* **2001**, *412*, 169.
(43) Luo, Q.; Zhu, H.; Zhou, Y.; Zheng, G.; Zhao, D. *J. Mater. Chem.* **2001**, *11*, 2934.
(44) Van Der Voort, P.; Ravikovitch, P. I.; De Jong, K. P.; Neimark, A. V.; Janssen, A. H.; Benjelloun, M.; Van Bavel, E.; Cool, P.; Weckhuysen, B. M.; Vansant, E. F. *Chem. Commun.* **2002**, 1010.
(45) Van Der Voort, P.; Ravikovitch, P. I.; De Jong, K. P.; Benjelloun, M.; Van Bavel, E.; Janssen, A. H.; Neimark, A. V.; Weckhuysen, B. M.; Vansant, E. F. *J. Phys. Chem. B* **2002**, *106*, 5873.
(46) Van Der Voort, P.; Ravikovitch, P. I.; Neimark, A. V.; Benjelloun, M.; Van Bavel, E.; De Jong, K. P.; Weckhuysen, B. M.; Vansant, E. F. *Stud. Surf. Sci. Catal.* **2002**, *141*, 45.
(47) Janssen, A. H.; Van Der Voort, P.; Koster, A. J.; de Jong, K. P. *Chem. Commun.* **2002**, 1632.
(48) Shin, H. J.; Ryoo, R.; Kruk, M.; Jaroniec, M. *Chem. Commun.* **2001**, 349.
(49) Ryoo, R.; Joo, S. H.; Kruk, M.; Jaroniec, M. *Adv. Mater.* **2001**, *13*, 677.
(50) Kim, S.-S.; Pinnavaia, T. J. *Chem. Commun.* **2001**, 2418.
(51) Joo, S. H.; Ryoo, R.; Kruk, M.; Jaroniec, M. *J. Phys. Chem. B* **2002**, *106*, 4640.
(52) Lee, J.-S.; Joo, S. H.; Ryoo, R. *J. Am. Chem. Soc.* **2002**, *124*, 1156.
(53) Kang, M.; Yi, S. H.; Lee, H. I.; Yie, J. E.; Kim, J. M. *Chem. Commun.* **2002**, 1944.
(54) Lu, A.-H.; Schmidt, W.; Taguchi, A.; Spliethoff, B.; Tesche, B.; Schuth, F. *Angew. Chem., Int. Ed.* **2002**, *41*, 3489.
(55) Sing, K. S. W.; Everett, D. H.; Haul, R. A. W.; Moscou, L.; Pierotti, R. A.; Rouquerol, J.; Siemieniewska, T. *Pure Appl. Chem.* **1985**, *57*, 603.
(56) Kruk, M.; Jaroniec, M. *J. Phys. Chem. B* **2002**, *106*, 4732.
(57) Kruk, M.; Jaroniec, M. *Chem. Mater.* **2000**, *12*, 222.
(58) Jaroniec, M.; Kruk, M.; Olivier, J. P. *Langmuir* **1999**, *15*, 5410.
(59) Kruk, M.; Jaroniec, M.; Gadkaree, K. P. *J. Colloid Interface Sci.* **1997**, *192*, 250.

(60) Barrett, E. P.; Joyner, L. G.; Halenda, P. P. *J. Am. Chem. Soc.* **1951**, *73*, 373.
(61) Kruk, M.; Jaroniec, M.; Sayari, A. *Langmuir* **1997**, *13*, 6267.
(62) Sayari, A.; Kruk, M.; Jaroniec, M. *Catal. Lett.* **1997**, *49*, 147.
(63) Matos, J. R.; Mercuri, L. P.; Kruk, M.; Jaroniec, M. *Chem. Mater.* **2001**, *13*, 1726.
(64) Kim, J. M.; Sakamoto, Y.; Hwang, Y. K.; Kwon, Y.-U.; Terasaki, O.; Park, S.-E.; Stucky, G. D. *J. Phys. Chem. B* **2002**, *106*, 2552.
(65) Kipkemboi, P.; Fogden, A.; Älfredsson, V.; Flodstrom, K. *Langmuir* **2001**, *17*, 5398.
(66) Kruk, M.; Jaroniec, M. *Chem. Mater.*, submitted.
(67) Kruk, M.; Jaroniec, M. *Chem. Mater.* **2001**, *13*, 3169.
(68) Matos, J. R.; Mercuri, L. P.; Kruk, M.; Jaroniec, M. *Langmuir* **2002**, *18*, 884.
(69) Ravikovitch, P. I.; Neimark, A. V. *Langmuir* **2002**, *18*, 1550.
(70) Kruk, M.; Antochshuk, V.; Matos, J. R.; Mercuri, L. P.; Jaroniec, M. *J. Am. Chem. Soc.* **2002**, *124*, 768.
(71) Goltner, C. G.; Smarsly, B.; Berton, B.; Antonietti, M. *Chem. Mater.* **2001**, *13*, 1617.
(72) Smarsly, B.; Polarz, S.; Antonietti, M. *J. Phys. Chem. B* **2001**, *105*, 10473.
(73) Ryan, K. M.; Coleman, N. R. B.; Lyons, D. M.; Hanrahan, J. P.; Spalding, T. R.; Morris, M. A.; Steytler, D. C.; Heenan, R. K.; Holmes, J. D. *Langmuir* **2002**, *18*, 4996.
(74) Park, J. C.; Lee, J. H.; Kim, P.; Yi, J. in *Abstracts of 3rd International Mesostructured Materials Symposium*, July 8−11, 2002, PA-25, p 75.
(75) Cui, X.; Yoo, G.; Park, J.; Ahn, J.-H.; Zin, W.-C.; Cho, W.-J.; Ha, C.-S. in *Abstracts of 3rd International Mesostructured Materials Symposium*, July 8−11, 2002, PA-27, p 77.
(76) Monnier, A.; Schuth, F.; Huo, Q.; Kumar, D.; Margolese, D.; Maxwell, R. S.; Stucky, G. D.; Krishnamurty, M.; Petroff, P.; Firouzi, A.; Janicke, M.; Chmelka, B. F. *Science* **1993**, *261*, 1299.
(77) Cheng, C.-F.; Luan, Z.; Klinowski, J. *Langmuir* **1995**, *11*, 2815.
(78) Holmes, S. M.; Zholobenko, V. L.; Thursfield, A.; Plaisted, R. J.; Cundy, C. S.; Dwyer, J. *J. Chem. Soc., Faraday Trans.* **1998**, *94*, 2025.
(79) Bagshaw, S. A.; Prouzet, E.; Pinnavaia, T. J. *Science* **1995**, *269*, 1242.
(80) Boissiere, C.; Larbot, A.; Bourgaux, C.; Prouzet, E.; Burton, C. A. *Chem. Mater.* **2001**, *13*, 3580.
(81) Van Der Voort, P.; Benjelloun, M.; Vansant, E. F. *J. Phys. Chem. B* **2002**, *106*, 9027.